Development of an UAV prototype for visual inspection of aerial electrical lines

Walter Benitez *, Yessica Bogado*, Ariel Guerrero† and Mario Arzamendia‡
* Research Center of Science, Technology and Advanced Innovation (CICTIA)
"Our Lady of the Assumption" Catholic University (UCA) - Hernandarias, Paraguay
Email: walter.benitez@ucap.edu.py, yessica.bogado@ucap.edu.py
†Innovation Center in Automation and Control (CIAC)
Technology Park of Itaipu (PTI) - Hernandarias, Paraguay
Email: ariel.guerrero@pti.org.py
‡ Laboratory of Distributed Systems
Faculty of Engineering, National University of Asuncion (FIUNA) - Asuncion, Paraguay
Email:marzamendia@ing.una.py

***Abstract*—The development of an attitude and altitude control system of an unmanned aerial vehicle for visual inspection of aerial electrical lines is presented. The system was implemented using quaternions algebra and the altimeter equation for the orientation estimation with the purpose of controlling the quadcopter. The proposed system was simulated in Matlab using a Newton-Euler model and compared with the performance on a real prototype operation, obtaining similar results in both cases.**

***Keywords*—aerial electrical lines, visual inspection, quadrotor, control theory, quaternions.**

I. Introduction

The electrical line inspections play a very important role in maintaining the quality of the energy delivered because of its relation with the predictive and preventive maintenance. It is clear that electrical companies should implement new methods and techniques that allow the routinely realization of such inspections avoiding as much as possible urgent maintenance tasks that require the interruption of the energy provision. The responsible institutions for the transmission and distribution of electrical energy use different inspection methods for controlling the state of the electrical lines and its accessories. The visual inspection consist of a meticulous task where physical damages are searched or possible difficulties that may reduce the efficiency of the electrical system. Diverse problems may be found when inspecting the lines, for example, at the insulating chains leakage lines may appear, insulating loss, breakage or cracking of the bells as well as loss of galvanized, rust, appearance of flakes or bubbles at the ironwork; even it is possible to see other inconveniences as damage by organic material, weather damage, the sliding of the shock absorber or invasion of the vegetation [1]. Visual inspection is an activity that accompanies the predictive maintenance with the objective of predicting failures and take preventive and/or corrective actions, keeping the conditions safe and preventing accidents [2]. There are four visual inspection techniques: foot patrol, climbing robots, manned aerial vehicles and unmanned aerial vehicles [3] [4]. The foot patrol is the most economical type and with the least risk because the lines are simply inspected from the ground with the support of binoculars. However the procedure is slow and the diagnosis is less precise. The manned aerial vehicles, specifically the helicopters, allow advantages as the speed and accessibility to irregular terrains, however the high costs and the danger exposures by the approximation of the operators with live lines do not allow their use commonly [3]. A more modern style is the use of climbing robots which offer a more precise inspection due to its proximity of the targets, but its complexity in the development for overcome obstacles, the effects of electromagnetic field over its sensors and electronics parts do not make them an economical solution. Currently the use of robotics platforms for observation is a growing interest field for many companies and institutions. A visual inspection using UAV (Unmanned Aerial Vehicle) are faster, more versatile and more economical [3] [4] [5]. These vehicles offer the capacity of stationary flight for a better image capture from different points around the electrical lines without putting the life of operators in risk. The UAVs or drones are vehicles that do not need a crew on them to control or conclude a specific task. It might be defined as robotic systems that land from a ground base and are controlled remotely by pilots, or autonomously following a mission previously programmed; or even both instances can be combined. The characteristics and costs vary according to the application, which it can be for environmental monitoring, search task, facilities supervision, surveillance, etc. The UAV may be catalogued according to different aspects, for example the flying capacity (autonomy), application or type of aircraft [6]. In the present work the UAV known as quadrotor is employed. The first step of this work is to study the mathematical modeling of the UAV which considers the aerodynamical effects of the vehicle. Currently, there are different variety of models [7] [8] [9] [10]. Defining an appropriate model plays an important role at the time of designing the control system and performing the simulation studies. The control assumes the availability of the variables of state, i.e., the estimation of the vehicle orientation. There

are different control algorithms due to the fact that the model of the quadrotor is multivariable and not lineal. Among the available bibliography of the topic, Schermuk [7] analyze the difference between the representations with Euler angles and quaternions, expose the advantages of the trajectory following around the main axis (eigenaxis) and finishes with a comparison between a PID (Proportional Integral Derivative) control and the LQR (Linear Quadratic Regulator). Bresciani [8] introduces with details a model based on the laws of Newton with the representation in Euler angles and its relationship with the DCM (Direction Cosine Matrix). On the other hand Fresk [9] proposed a control scheme based on quaternions, where an attitude model and a square non-lineal proportional control algorithm were implemented, both in the quaternions space without transformations and calculations with the Euler angles. In the present work the simulation, building and implementation of an UAV is done, applying a CAS (Control Augmented System) + SAS (Stability Augmented System) with quaternions algebra that later is verified by using it for a visual inspection of an aerial electrical line.

The rest of the paper is organized as follows, in Section II the definition of quaternions is presented and used to define a Newton-Euler model to describe the movement of the quadcopter. Section III presents the design of the control system (altituted and attitude) using the concepts of Section II. In Section IV, the quadcopter prototype built is described; Section V presents the results of simulating the control system in Matlab and Section VI the measurements of the performance of the control system during operation of the prototype. Finally, Section VI presents the conclusion and future work to be done.

II. Theoretical Framework

The theoretical framework is divided into two parts: the dynamic model that is related to the physical behavior of the aircraft and the representation of the attitude of it in space, which was made with Euler angles because they are much more intuitive for interpreting the equations in the simulation; and quaternions which is another way to represent the attitude of the aircraft that was used to implement control over it to avoid the problem of gimbal lock produced by the Euler angles [7].

A. Quaternions

The quaternions is a four dimensional hypercomplex number that can be used to represent an orientation of a body frame in 3D space. A quaternion Q have the following form $q_0 + q_1 i + q_2 j + q_3 k$, where q_0, q_1, q_2, q_3 are real numbers called components of the quaternion and i, j, k are imaginary units.

For rotation the quaternion has the following form [11]

$$Q = (\cos\frac{\alpha}{2}, \sin\frac{\alpha}{2}\hat{r}) \tag{1}$$

Where: $q_0 = \cos(\frac{\alpha}{2})$, $q_1 = \sin(\frac{\alpha}{2})\, r_x$, $q_2 = \sin(\frac{\alpha}{2})\, r_y$, $q_3 = \sin(\frac{\alpha}{2})\, r_z$

The angle α represents the magnitude to be rotated around the main axis r, defined as eigenaxis in Euler's rotation theorem. Just as the property of orthogonal matrices rotation [6], quaternion rotation obey the following [7]:

$$Q_C^A = Q_B^A . Q_C^B \tag{2}$$

$$(Q_B^A)^* = (Q_B^A)^{-1} = Q_A^B \tag{3}$$

Were $(Q_B^A)^*$ is the conjugated quaternion of Q_B^A

Also being $\hat{r} \in \mathbb{R}^{3\times1}$ the rotation axis of the quaternion Q and α the rotation angle, the following is allowed [7]:

$$\ln Q = \frac{\hat{r}\alpha}{2} \tag{4}$$

Considering the quaternion rotation it can be defined a rotation matrix with the components of the quaternion [12]:

$$\begin{bmatrix} q_0^2+q_1^2-q_2^2-q_3^2 & 2(q_1q_2-q_3q_0) & 2(q_0q_2+q_1q_3) \\ 2(q_1q_2+q_3q_0) & q_0^2-q_1^2+q_2^2-q_3^2 & 2(q_2q_3+q_1q_0) \\ 2(q_1q_3-q_2q_0) & 2(q_0q_1-q_2q_3) & q_0^2-q_1^2-q_2^2+q_3^2 \end{bmatrix}$$

By combining the property of quaternions with the sequence of rotation 3,2,1 established in Euler angles it can be stated that

$$Q_{Euler} = Q_\psi Q_\theta Q_\phi = \begin{bmatrix} \cos\frac{\psi}{2} \\ 0 \\ 0 \\ \sin\frac{\psi}{2} \end{bmatrix} \begin{bmatrix} \cos\frac{\theta}{2} \\ 0 \\ \sin\frac{\theta}{2} \\ 0 \end{bmatrix} \begin{bmatrix} \cos\frac{\phi}{2} \\ \sin\frac{\phi}{2} \\ 0 \\ 0 \end{bmatrix} \tag{5}$$

Equation (6) presents the conversion of quaternion to Euler angles [12]:

$$\begin{bmatrix} \phi \\ \theta \\ \psi \end{bmatrix} = \begin{bmatrix} \arctan\left(\frac{2(q_0q_1+q_3q_2)}{1-2(q_1^2+q_2^2)}\right) \\ \arcsin\left(2(q_0q_2+q_3q_1)\right) \\ \arctan\left(\frac{2(q_0q_3+q_1q_2)}{1-2(q_2^2+q_3^2)}\right) \end{bmatrix} \tag{6}$$

B. Dynamic Model

According to Bresciani [8] there are four types of basic movements for a quadcopter: Sustentation (U_1), Roll (U_2), Pitch (U_3) and Yaw (U_4). These movements are represented in equations as the forces that drive themselves to implement these actions. Considering these four movements, the system dynamics and the direction cosine matrix we have a model called Newton - Euler and it is described by these equations:

$$\begin{aligned} \ddot{x} &= \frac{U_1}{m}(\sin(\psi)\sin(\phi) + \cos(\psi)\sin(\theta)\cos(\theta)) \\ \ddot{y} &= \frac{U_1}{m}(-\cos(\psi)\sin(\phi) + \sin(\psi)\sin(\theta)\cos(\theta)) \\ \ddot{z} &= \frac{U_1}{m}\cos(\theta)\cos(\phi) - g \\ \dot{p} &= \frac{I_{YY}-I_{ZZ}}{I_{XX}}qr - \frac{I_{TA}}{I_{XX}}q\Omega_t + \frac{U_2}{I_{XX}} \\ \dot{q} &= \frac{I_{ZZ}-I_{XX}}{I_{YY}}pr - \frac{I_{TA}}{I_{YY}}p\Omega_t + \frac{U_3}{I_{XX}} \\ \dot{r} &= \frac{I_{XX}-I_{YY}}{I_{ZZ}}pq + \frac{U_4}{I_{ZZ}} \end{aligned} \tag{7}$$

As x, y, z represent the position in space, $\omega = [p, q, r]$ the angular velocity according to the vehicle body frame,

$I_{XX}, I_{YY}, I_{ZZ}, I_{TA}$ inertial moments of the vehicle and U_1, U_2, U_3, U_4 are the forces and moments described above. Then these forces are related to the rotation speed of the propellers by the following equations.

$$\begin{aligned} U_1 &= b(\Omega_1^2 + \Omega_2^2 + \Omega_3^2 + \Omega_4^2) \\ U_2 &= bl(-\Omega_1^2 - \Omega_2^2 + \Omega_3^2 + \Omega_4^2) \\ U_3 &= bl(-\Omega_1^2 + \Omega_2^2 + \Omega_3^2 - \Omega_4^2) \\ U_4 &= d(-\Omega_1^2 + \Omega_2^2 - \Omega_3^2 + \Omega_4^2) \\ \Omega_t &= -\Omega_1 + \Omega_2 - \Omega_3 + \Omega_4 \end{aligned} \tag{8}$$

Where $\Omega_n (n = 1, 2, 3, 4)$ represents the rotation of each propeller and its unit is rad/sec, Ω_t is the sum of all speed rotations, b is the thrust factor, d is the drag factor and l is the distance between the center of the motor to the center of quadcopter body.

III. Design of the Control System

Generally aircraft control systems can be classified into a SAS, CAS and an autopilot system. The stability augmentation system (SAS) aims to stabilize the vehicle controlling the dynamics (angular speed) while the control augmentation system (CAS) aims to maintain a desired orientation [7].

In order to make a simple control design and linearly independent on each degree of freedom the Newton - Euler model (7) is simplified as follows.

$$\begin{aligned} \ddot{x} &= \frac{U_1}{m}(\sin(\psi)\sin(\phi) + \cos(\psi)\sin(\theta)\cos(\theta)) \\ \ddot{y} &= \frac{U_1}{m}(-\cos(\psi)\sin(\phi) + \sin(\psi)\sin(\theta)\cos(\theta)) \\ \ddot{z} &= \frac{U_1}{m}\cos(\theta)\cos(\phi) - g \\ \dot{p} &= \frac{U_2}{I_{XX}} \\ \dot{q} &= \frac{U_3}{I_{XX}} \\ \dot{r} &= \frac{U_4}{I_{ZZ}} \end{aligned} \tag{9}$$

And to use the four basic movements as input signals an open loop control is applied with the inverse of (8).

$$\begin{aligned} \Omega_1^2 &= \frac{U_1}{4b} - \frac{U_2}{4bl} - \frac{U_3}{4bl} - \frac{U_4}{4d} \\ \Omega_2^2 &= \frac{U_1}{4b} - \frac{U_2}{4bl} + \frac{U_3}{4bl} + \frac{U_4}{4d} \\ \Omega_3^2 &= \frac{U_1}{4b} + \frac{U_2}{4bl} + \frac{U_3}{4bl} - \frac{U_4}{4d} \\ \Omega_4^2 &= \frac{U_1}{4b} + \frac{U_2}{4bl} - \frac{U_3}{4bl} + \frac{U_4}{4d} \end{aligned} \tag{10}$$

A. Attitude Control

For attitude control we proceeded to choose a CAS + SAS dual control (Fig. 1) because of its wide use in the field of UAVs [10]. For CAS a proportional approach was used and for SAS a PIDT1 (Proportional, Integral, Derivative with a low-pass filter) [13].

The error is obtained through the rotation needed to go from current quaternion (Q_a) to desired quaternion (Q_{des}), such

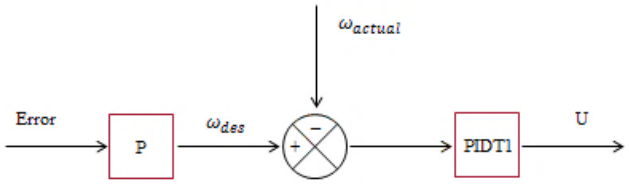

Fig. 1. Block diagram of CAS+SAS control

rotation obtained through (3) is represented by the quaternion error as follows:

$$Q_{error} = Q_a^* . Q_{des} \tag{11}$$

Where Q_a^* is the conjugated of Q_a.

Then from (4):

$$2 \ln Q_{error} = 2 \ln(Q_a^* . Q_{des}) = \hat{r}\alpha \tag{12}$$

As the components of $\hat{r}\alpha$ vector represents the error in each main axis [7] [14] [9].

$$E_x = r_x \alpha \tag{13}$$

$$E_y = r_y \alpha \tag{14}$$

From this the error for X and Y axis is obtained, however there is a problem with the Z axis because the DMP (Digital Motion Processor), which is in charge of fusing the data of the IMU (Inertial Motion Unit, MPU6050), does not fuse the data taken from the magnetometer. A solution to this is given by using ψ_{false}, calculated with the formula obtained in (6) with Q_a.

$$\psi_{false} = \arctan\left(\frac{2(q_0 q_3 + q_1 q_2)}{1 - 2(q_2^2 + q_3^2)}\right) \tag{15}$$

The desired quaternion (Q_{des}) is obtained using (5) with ψ_{false} and desired rotation angles in the X and Y axis.

With this it only remains to consider the error of the Z axis and for that a complementary filter is applied on the orientation obtained through magnetometer (17) [15] and gyroscope (rdt) as showed on (16). After that the error is calculated with ψ_{des} (18).

$$\psi_{real} = \rho(\psi_{real} + rdt) + \psi_{mag}(1 - \rho) \tag{16}$$

$$\psi_{mag} = \arctan\left(\frac{m_x}{m_y}\right) \tag{17}$$

$$E_z = \psi_{des} - \psi_{real} \tag{18}$$

Where m_x and m_y are the values obtained with the magnetometer of the magnetic field of the earth according to the X and Y axis and have to be calculated correctly and rotated to the inertial frame with the current quaternion. And ρ>0 is a constant that indicates the contribution of the gyroscope to ψ_{real} and it has a maximum value of 1.

B. Altitude Control

The height control is highly related to the "hovering", i.e. keeping the altitude in a certain height and holding the attitude without motion in a horizontal position relative to the ground [10]. As in attitude control, to perform the control action we proceeded to work with the same strategy of dual control, a CAS to control the position of the quadcopter according to a reference value and SAS to vary the quadcopter thrust according to a desired vertical speed [16] as seen in Fig. 2.

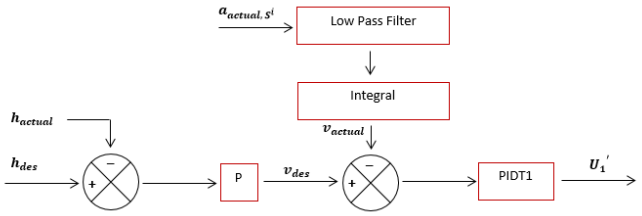

Fig. 2. Block diagram of altitude control

The estimation of values is necessary, the current height is obtained through barometer with the altimeter equation (21) [17], and then filtered with a low pass filter that is related to the speed v_{actual} ((22) and (6)). To obtain the speed first accelerometer data must be passed to the inertial frame, subtracting the values of gravity so as to be able to measure the acceleration without the influence of gravity as it shows in (20). Then these data is filtered with LPF (Low Pass Filter) of 50 Hz and proceeds to integration.

$$U_1 = mg + U_1' \tag{19}$$

$$a_{actual,S^i} = (a_{actual} - g_z)_{v3 \to S^i} \tag{20}$$

$$z = \frac{T_0}{\Gamma}\left[1 - \left(\frac{P}{P_0}\right)^{\frac{R_{spe} \cdot \Gamma}{g}}\right] \tag{21}$$

$$KP_1 = p(1 - e^{C_1|v_{actual}|}) \tag{22}$$

$$\begin{aligned} h_{actual_n} &= (z - z_0)(KP_1 + 1 - p) \\ &+ (h_{actual_{n-1}})(p - KP_1) \end{aligned} \tag{23}$$

Where p is a value ranging from 0 to 1 that regulates the dependency of the current reading in relation to a previous one, C_1 is a negative value that regulate the dependency of the filter to the vertical speed of the aircraft and $v3 \to S^i$ represents the rotation from the body frame to inertial frame [6]. This filter is made to counteract the variation produced by the barometer when the aircraft hovers.

For the altimeter equation we have that R_{spec} is the specific constant of gas, P_0 is the pressure at sea level, P is the actual pressure, T_0 is the temperature at sea level and Γ is the slop for the uniform decrease of temperature relative to height. The reference height for quadcopter is z_0.

C. General Control Scheme

Once the sectors of the control system were developed they are connected to each other according to the Fig. 3. In the figure can be seen that is possible to choose a type of control either manually or automatically. If the manual control is selected, the user manipulates the force values and the desired tilt angles; on the other hand, the automatic control maintains the height or position by GPS and barometer. After this, it is passed to the SAS + CAS control and the four basic movements (U_1, U_2, U_3, U_4) are obtained and used in (10) to get the desired rotation. Getting with it the PWM needed to regulate the ESC to finally feedback all the control blocks through the sensors.

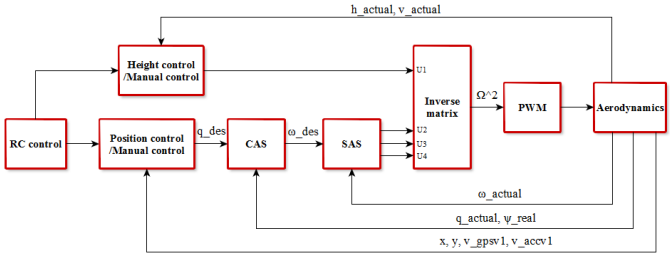

Fig. 3. General Control Scheme

IV. Hardware Description

The prototype is a quadcopter Fig. 4, the motors used are BLDC (Brushless Direct Current) type of 935 KV, which are three-phase motors that feed on a DC continuous source, the advantage of these engines is that they are lighter, more dynamic and more response efficient; the propellers are 10x4.5 inches. An ESC (Electonic Speed Control) 30 A was used for controlling the BLDC motors., this driver is also responsible for supplying power to the electronic components of UAVs. The main power source is a rechargeable LiPo (Lithium Polymer) 3S 5000 mAh 25C, which is a lightweight battery with a reduced volume. An eight channel radio control with PPM (Pulse Position Modulation) was used to operate the quadcopter, and covers distances up to 1.5 km and operates at a frequency of 2.4 GHz. The main element of the vehicle is the flight controller Crius AIOP (All in One Pro) v2.1, this electronic board has built-in various sensors like a gyroscope / accelerometer MPU6050 6-axis high precision altimeter MS5611-01BA01 and HMC5883L 3-axis magnetometer. The integrated microcontroller ATMEGA 2560 is an 8-bit, 16 MHz and communicates with external devices via the pins and serial ports. Two wireless modules (2.4 GHz) were used to transmit data from the flight controller to the ground station. In order to display in a computer the quadcopter objective a transmitter audio and video receptor of 500mW power operating at a frequency of 5.8 GHz was chosen and brings a CCD camera(Charge Coupled Device) with it. The power supply of the transmitter and receiver is a 1300 mAh LiPo battery for each. It also had incorporated a GPS module (Global Positioning System) to know the quadcopter's position. The total budget of this prototype was about 700 U$ FCA (Free Carrier).

V. Simulation and Implementation of Control

Simulations were performed using Matlab(Version R2013b) with the previously described model [8] [18], the adopted parameters were as follows:

Fig. 4. Prototype

TABLE I
PARAMETERS OF THE PHYSICAL MODEL

Name	Symbol	Value
Quadcopter's Mass	M	$1.48\,kg$
Thrust coefficient	b	$12.76 \times 10^{-6}\ N.s^2/rad^2$
Drag coefficient	d	$1.07 \times 10^{-6}\ N.m.s^2/rad^2$
Quadcopter's radius	l	$0.23\,m$
Inertia relative to the X axis	I_{XX}	$9.86 \times 10^{-3}\ kg.m^2$
Inertia relative to the Y axis	I_{YY}	$9.86 \times 10^{-3}\ kg.m^2$
Inertia relative to the Z axis	I_{ZZ}	$16.64 \times 10^{-3}\ kg.m^2$
Total inertia of the actuators	I_{TA}	$74.12 \times 10^{-6}\ kg.m^2$

TABLE II
CONTROL PARAMETERS

CAS			
	Type	**Symbol**	**Value**
Attitude	Proportional	KP_ϕ	3
		KP_θ	3
		KP_ψ	2
Altitude	Proportional	KP_h	1
SAS			
	Type	**Symbol**	**Value**
Attitude	Proportional	KP_ϕ	0.75
		KP_θ	0.75
		KP_ψ	0.75
	Integral	KI_ϕ	0.35
		KI_θ	0.35
		KI_ψ	0.21
	Derivative	KD_ϕ	0.01
		KD_θ	0.01
		KD_ψ	0.01
Altitude	Proportional	KP_h	2.9
	Integral	KI_h	0.3
	Derivative	KD_h	0.0015

Two simulations were executed, one assuming that the sensors are ideal and another with disturbance. In attitude control, a reference value of 20° was choose and when sensors are ideal results show an almost nonexistent peak and a rise time of about 0.89 seconds as shows in Fig. 5. On the other hand when input a Gaussian noise of 5% of the value taken by the sensors the results shows a standard deviation of 0.43 degrees in the roll, 0.49 degrees on yaw and 0.54 degrees in the pitch, the values of overshoot and time rise are held as in Fig. 6.

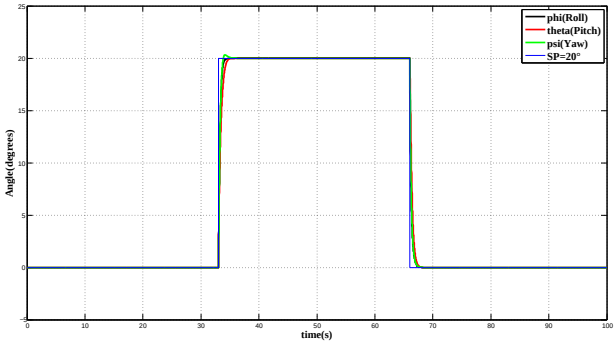

Fig. 5. Step response of the Yaw, Pitch and Roll angles without noise

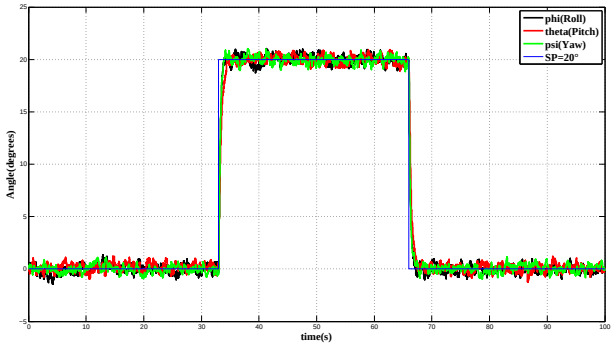

Fig. 6. Step response of the Yaw, Pitch and Roll angles with noise

At the height control reference value of 2 meters was used, for a simulation without disturbing the rise time is 2.5 seconds and with an overshoot less than 10% as it can be seen in Fig. 7. The simulation with Gaussian noise of 10% of the real value produced a standard deviation of 0.022 meters showing in Fig. 8.

VI. EXPERIMENTAL RESULTS

The Table III shows the contrast of standard deviations relative to a reference value between flight simulations performed previously and real stationary flights with the prototype.

The values of both, roll and pitch, are similar to the simulation results and the value of yaw differs mainly because of electromagnetic disturbance that motors produce in the magnetometer. As for height, pressure variations produced a standard deviation of 0.17 meters in hovering. It is necessary to note that rates estimated with the accelerometer increases the amount of error in the controller.

After contrast, the inspection of a medium voltage transformer in an overhead power line was carried out (Fig. 9). Quadcopter position was about 7 meters above ground and about 5 meters from the transformer and no undesirable effects

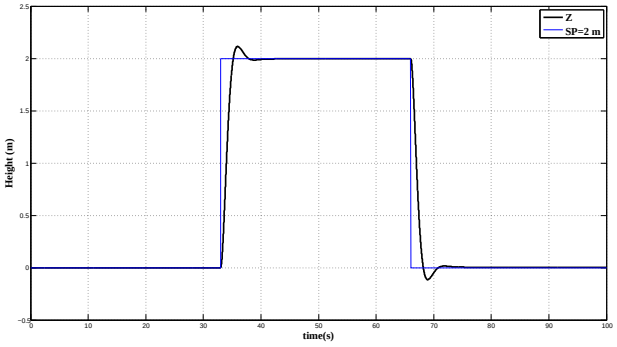

Fig. 7. Step response of altitude control without noise

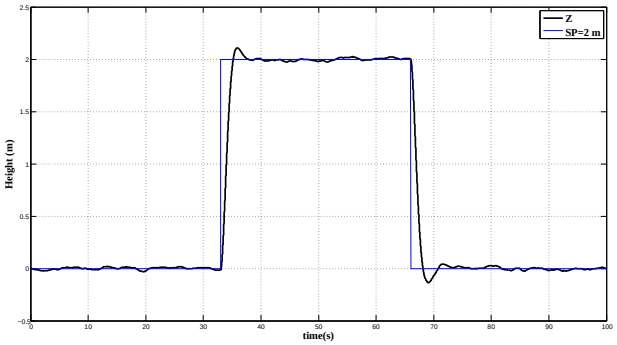

Fig. 8. Step response of altitude control with noise

Fig. 9. Visual inspection with the prototype seen from the ground

TABLE III
CONTRAST TABLE

	Simulated Test	**Real Test**
Roll (Degrees)	0.43	0.45
Pitch (Degrees)	0.54	0.41
Yaw (Degrees)	0.49	1.59
Height (meters)	0.02	0.17

were detected due to electromagnetic fields. The images were captured with the camera described before in section IV and transmitted from quadcopter to a computer on the ground.

VII. CONCLUSION

This paper presented a CAS + SAS (P + PIDT1) control system with the use of quaternion for UAV. The simulation of this system showed satisfactory results when comparing with the work of Bresciani, Kharsansky and Schermuk [8] [10] [7]. Finally, the prototype was used to perform the visual inspection of a medium voltage transformer in a power distribution line.

As future work, the following topics are suggested:

- Using extended Kalman filter with a more powerful microcontroller and to make a better estimate of the velocities and positions
- Implementing a tracking system for automated inspection
- Performing the contrast with other types of attitude and altitude control for UAVs
- When conducting inspections on transmission towers take into account the electromagnetic effect produced by high voltages and properly protect electronics of the UAV
- Studying and implementing the use of a thermal camera to identify hot spots

REFERENCES

[1] J. Boza, "Inspección integral de las líneas de transmisión," *Ingeniería Energética*, vol. 24, no. 3, pp. 3–7, 2003.
[2] DISPAC, "Manual de mantenimiento para redes eléctricas alta media y baja tensión," Quibd, 2015.
[3] J. Garcés, "Inspecciones aéreas de líneas de transmisión con alta tecnología," in *Jornadas Técnicas ISA*, 2012.
[4] J. León and M. C., "Estudio de soluciones existentes en el mercado para la inspección y manteniemiento de líneas eléctricas de alta tensión." Universidad Politécnica de Madrid, 2013.
[5] R. Gouws, "Prototype monitoring system for power line inspection by means of a pandaboard," *Journal of Energy and Power Engineering*, vol. 8, pp. 176–182, 2013.
[6] R. Austin, *Unmanned aircraft systems*. Chichester: John Wiley and Sons Ltd, 2010.
[7] D. Schermuk, "Diseño e implementación de un controlador para la orientación de un quadrotor," Facultad de Ingeniería de la Universidad de Buenos Aires, 2012.
[8] T. Bresciani, "Modelling, identification and control of a quadrotor helicopter," Master's thesis, Lund University, 2008.
[9] E. Fresk, "Full quaternion based attitude control for a quadrotor," in *European Control Conference (ECC)*, Zrich, 2013.
[10] A. Kharsansky, "Diseño e implementación de un sistema embebido de control de actitud para aeronaves no tripuladas," Facultad de Ingeniería de la Universidad de Buenos Aires, 2013.
[11] G. Torres del Castillo, "La representación de rotaciones mediante cuaterniones," *Miscelanea Matemtica*, pp. 43–50, 1999.
[12] M. Henderson, "Euler angles, quaternions, and transformation matrices," NASA, Houston, Texas, Tech. Rep., 1977.
[13] I. V. Airde. (2012) Attitude control structure, changing from pi to pid? diydrones.com. [Online]. Available: www.diydrones.com/forum/topics/attitude-control-structure-changing-from-pi-to-pid
[14] B. Michini, "Modeling and adaptive control of indoor unmanned aerial vehicles," Massachusetts Institute of Technology, 2009.
[15] Honeywell. (1995) Compass heading using magnetometers. [Online]. Available: www51.honeywell.com/aero/common/documents/myaerospacecatalog-documents/Defense_Brochures-documents/Magnetic__Literature_Application_notes-documents/AN203_Compass_Heading_Using_Magnetometers.pdf
[16] A. Copter. (2015) Altitude hold mode. [Online]. Available: copter.ardupilot.com/wiki/altholdmode
[17] D. of Mathematical Physics of the University College Dublin. (2005) The hydrostatic equation. [Online]. Available: maths.ucd.ie/met/msc/fezzik/Phys-Met/Ch03-Slides-2.pdf
[18] M. Ai-Omari, "Integrated simulation platform for indoor quadrotor applications," in *Mechatronics and its Applications (ISMA)*, Amman, 2013.